Bone Reports 12 (2020) 100251

Contents lists available at ScienceDirect

Bone Reports

journal homepage: www.elsevier.com/locate/bonr

# GLP-2 administration in ovariectomized mice enhances collagen maturity but did not improve bone strength

B. Gobron[a,b], B. Bouvard[a,b], E. Legrand[a,b], D. Chappard[a,c,d], G. Mabilleau[a,c,d,*]

[a] Groupe études remodelage osseux et biomatériaux, GEROM, UPRES EA4658, UNIV Angers, SFR 42-08, Institut de Biologie en Santé, CHU d'Angers, 49933 Angers cedex, France
[b] Service de Rhumatologie, CHU d'Angers, 49933 Angers cedex, France
[c] Service commun d'imageries et d'analyses microscopiques, SCIAM, UNIV Angers, SFR 42-08, Institut de Biologie en Santé, CHU d'Angers, 49933 Angers cedex, France
[d] UF de Pathologie osseuse, CHU d'Angers, 49933 Angers cedex, France

ARTICLE INFO

*Keywords:*
GLP-2
Bone remodeling
Bone strength
Bone composition
Infrared imaging

ABSTRACT

Osteoporosis and bone fragility are progressing worldwide. Previous published literature reported a possible beneficial role of gut hormones, and especially glucagon-like peptide-2 (GLP-2), in modulating bone remodeling. As now ($Gly^2$)GLP-2 is approved in the treatment of short bowel syndrome, we thought to investigate whether such molecule could be beneficial in bone fragility.

MC3T3 and Raw 264.7 were cultured in presence of ascending concentrations of ($Gly^2$)GLP-2. Collagen crosslinks, maturity, lysyl oxidase activity and osteoclastogenesis were then analyzed. Furthermore, ($Gly^2$)GLP-2, at the clinical approved dose of 50 µg/kg/day, was also administered to ovariectomized Balb/c mice for 8 weeks. Hundred µg/kg zoledronic acid (once iv) was also used as a positive comparator. Bone strength, microarchitectures and bone tissue composition were analyzed by 3-point bending, compression test, microCT and Fourier transform infrared imaging, respectively.

In vitro, ($Gly^2$)GLP-2 was potent in enhancing bone matrix gene expression but also to dose-dependently enhanced collagen maturation and post-processing. ($Gly^2$)GLP-2 was also capable of reducing dose-dependently the number of newly generated osteoclasts. However, in vivo, ($Gly^2$)GLP-2 was not capable of improving neither bone strength, at the femur diaphysis or lumbar vertebrae, nor bone microarchitecture. On the other hand, at the tissue material level, ($Gly^2$)GLP-2 significantly enhances collagen maturity and reduce phosphate/amide ratio.

Overall, this study highlights that despite modification of bone tissue composition, ($Gly^2$)GLP-2, at the clinical approved dose of 50 µg/kg/day, did not provide real beneficial effects in improving bone strength in a mouse model of bone fragility. Further studies are recommended to validate the best dose and regimen of administration to significantly enhance bone strength.

## 1. Introduction

Osteoporosis is defined as a systemic skeletal disease characterized by low bone mass and microarchitectural deterioration of bone tissue, with a consequent increase in bone fragility and susceptibility to fracture (*Am. J. Med.*, 1993). To prevent osteoporosis several therapies have been developed. In one side, antiresorptive drugs inhibit the activity of osteoclasts and this class is represented by bisphosphonates, selective estrogen receptor modulators or anti-RANKL. In the other side, anabolic drugs, as teriparatide, abaloparatide or romosozumab, increase bone formation. Taken together, these therapies permit to decrease vertebral fracture incidence by ~70% and non-vertebral fractures by ~50%, in postmenopausal women (McClung et al., 2013; Khosla et al., 2012; Ettinger et al., 1999; Neer et al., 2001; Cummings et al., 2009). These drugs are efficient but not perfect and none of them is specialized in the improvement of matrix quality (Boskey, 2013). However, in osteoporosis, modification of bone microarchitecture, microdamage accumulation and bone matrix composition, is important for optimal bone strength (Chappard et al., 2011). The bone matrix is made of an organic phase, mostly composed of type I collagen, and a mineral phase, composed of substituted poorly-crystalline hydroxyapatite tablets (Boskey, 2013). Although not yet approved as a therapy in post-menopausal osteoporosis, gut hormones seem to influence the quality and composition of the bone matrix (Gaudin-Audrain et al., 2013; Mabilleau, 2017; Mabilleau et al., 2013; Mieczkowska et al., 2013).

Among all gut hormones, glucagon-like peptide-2 (GLP-2) seems

* Corresponding author at: GEROM-LHEA UPRES EA 4658, Institut de Biologie en Santé, Université d'Angers, 4 rue Larrey, 49933 Angers Cedex 09, France.
*E-mail address:* guillaume.mabilleau@univ-angers.fr (G. Mabilleau).

https://doi.org/10.1016/j.bonr.2020.100251
Received 28 November 2019; Received in revised form 3 February 2020; Accepted 4 February 2020
Available online 05 February 2020

interesting for the treatment of bone fragility. Despite expression of the GLP-2 receptor (GLP-2r) in the gastro-intestinal tract, gall bladder, vagus nerve, lung and the central nervous system, a role for this hormone in bone remodeling has been previously suggested by several studies (Brubaker, 2018; Henriksen et al., 2004; Henriksen et al., 2007; Henriksen et al., 2009). GLP-2 is co-secreted with GLP-1 and PYY by enteroendocrine L-cells mainly located in the distal part of the small intestine and in colon (Drucker et al., 2017). Intact GLP-2 is rapidly cleaved by dipeptidyl peptidase-4 (DPP-4), with a half-life in plasma of approximately 7 min (Hartmann et al., 2000). This degradation rate precluded the use of native GLP-2 as a possible therapy and led to the development of DPP-4-resistant GLP-2 analogues. The major analogue is represented by teduglutide, a ($Gly^2$)GLP-2 analogue that has recently been approved for the treatment of short bowel syndrome.

Henriksen et al. demonstrated that bone resorption is reduced after a meal and GLP-2 concentration is correlated with this decrease (Henriksen et al., 2003). Moreover, a single subcutaneous injection of GLP-2, in fasting postmenopausal women, induces a dose-dependent decrease in bone resorption markers (Henriksen et al., 2003). A single GLP-2 injection in healthy postmenopausal women also suppressed the nocturnal rise in CTx-I levels without impairing bone formation markers in the 6 h post-injection (Henriksen et al., 2004). These results were confirmed in longer time study, where a sustained administration for 14 days of a modified GLP-$2_{(1–34)}$ resulted in marked reduction in bone resorption but not bone formation (Henriksen et al., 2007). Four-month treatment with GLP-2 in postmenopausal women with mild osteopenia resulted in higher total hip and femoral neck bone mineral densities (BMD) (Henriksen et al., 2009). However, despite increases in femoral neck BMD, little is known on the impact of GLP-2 therapy on bone quality, an important contributor of bone strength.

The aim of the present study was to investigate the effect of ($Gly^2$)GLP-2, also known as teduglutide, in ovariectomized Balb/c mice on bone strength, mass and quality as a proof-of-concept to reposition teduglutide for the treatment of bone fragility.

## 2. Material and methods

### 2.1. Cells and reagents

MC3T3-E1 cells, subclone 4 (ATCC CRL-2593), and RAW 264.7 cells (ATCC TIB-71) were purchased from American Type Culture Collection (ATCC, Teddington, UK). ($Gly^2$)GLP-2 analogue was purchased from GeneCust with a purity > 95% (Boynes, France). Purity has been verified by high performance liquid chromatography and peptide composition validated by mass spectroscopy. Receptor activator of nuclear factor κB ligand (RANKL) was purchased from R&D Systems Europe (Abingdon, UK). Zoledronic acid was purchased from Tocris (Lille, France). All other chemicals were purchased from Sigma-Aldrich (Lyon, France) unless otherwise stated.

### 2.2. Cell culture

MC3T3-E1 cells were grown in propagation medium containing alpha minimum essential medium (αMEM) supplemented with 5% fetal bovine serum (FBS), 5% bovine calf serum, 100 UI/mL penicillin, and 100 µg/mL streptomycin in a humidified atmosphere enriched with 5% $CO_2$ at 37 °C.

For differentiation studies, cells were detached with trypsin-EDTA and plated at a density of $1.5 \times 10^4$ cells/$cm^2$ and grown to confluence in propagation medium. At confluence, the propagation medium was replaced by the differentiation medium containing αMEM supplemented with 5% FBS, 5% bovine calf serum, 100 U/ml penicillin, 100 µg/ml streptomycin, 50 µg/ml ascorbic acid and several concentrations of ($Gly^2$)GLP-2. All factors were replenished every 2 days. The day to which the propagation medium was switched to differentiation medium was considered as day 1. The differentiation medium was replenished every two days. Fourteen days later, osteoblast cultures were fixed in absolute ethanol, scrapped off the culture dish and transferred onto BaF2 windows where they were air-dried before being analyzed by Fourier transform infrared microspectroscopy (FTIRM) as described below for collagen maturity evaluation.

In order to generate osteoclasts, Raw 264.7 cells were plated at a concentration of $2.5 \times 10^5$ cells/ml in 24-well plate in alpha-MEM supplemented with 10% fetal calf serum (FCS), 2 mM L-glutamine, 100 U/ml penicillin, 100 µg/ml streptomycin, 10 ng/ml soluble murine RANKL and several concentrations of ($Gly^2$)GLP-2. After four and half days of culture, tartrate-resistant acid phosphatase (TRAcP) staining was performed as described below to evidence the presence of osteoclast cells.

### 2.3. Lysyl oxidase (LOX) activity

LOX activity was assessed in the cell culture supernatant and in the cell layer after 13 days of culture as reported previously (Mieczkowska et al., 2015). At day 12, the differentiation medium was replaced by phenol red-free DMEM containing 0.5% bovine serum albumin, 50 µg/ml ascorbic acid and various concentrations of ($Gly^2$)GLP-2. After 24 h, cell culture supernatants were collected, centrifuged at 3000 rpm for 30 min at 4 °C, aliquoted and stored at −80 °C until use. The cell layer was extracted in urea buffer as reported in Bedell-Hogan et al. (1993). Then, supernatants were incubated at 37 °C for 30 min in the presence of 1.2 M urea, 50 mM sodium borate (pH 8.2), 1.3 nmol $H_2O_2$, 1 UI/ml horseradish peroxidase, 10 mM diaminopentane, 10 µM Ampliflu™ red and ± 0.5 mM β-aminopropionitrile (BAPN) in opaque 96 well plates. At the end of the incubation period, the plate was placed on ice and fluorescence was read using a M2 microplate reader (Molecular devices, St Gregoire, France) with excitation and emission wavelength set up at 563 nm and 587 nm, respectively. As BAPN is a specific lysyl oxidase inhibitor, the residual amine oxidase activity evidenced in the presence of BAPN was subtracted from the activity observed in the absence of BAPN. Lysyl oxidase activity was reported as the fold change versus CTRL of the pooled supernatant and cell layer fractions.

### 2.4. Collagen fibrils examination

After 13 days of culture, osteoblasts and their produced extracellular matrix were rinsed with 0.2 M cacodylate buffer (pH 7.4) and fixed in 2.5% glutaraldehyde in cacodylate buffer. Then cultures were post-fixed with 1% osmium tetroxide/1% potassium ferrocyanide and dehydrated in a graded series of ethanol prior to embedding in epoxy resin. Ultrathin sections were cut with a diamond knife, contrasted with 3% uranyl acetate and observed with a Jeol JEM 1400 (Jeol, Croisy sur Seine, France) operating with an accelerating voltage of 120 keV and a magnification of ×100,000. Image analysis with shape descriptors was used to determine the diameter of cross-sectioned collagen fibrils as previously described (Mieczkowska et al., 2015). Fibril sections with an aspect ratio < 1.2 were considered with low probability of local tilting. The minor diameter of fitted ellipse was selected as the value of fibril diameter as described by Starborg et al. (2013). More than 800 fibrils were measured per replicate and the mean fibril diameter has been computed and reported.

### 2.5. Collagen maturity evaluation

For collagen crosslink analysis in osteoblast cultures, extracellular matrix was fixed in absolute ethanol for 15 min, scrapped off the culture dish and transferred onto $BaF_2$ windows where it was air-dried. Integrity of the collagen extracellular matrix was verified by comparing the obtained mid-infrared spectrum with those of commercial collagen. Spectral analysis was performed using a Bruker Vertex 70 spectrometer (Bruker optics, Ettlingen, Germany) interfaced with a Bruker Hyperion 3000 infrared microscope equipped with a standard single element

Mercury Cadmium Telluride (MCT) detector. Mid-infrared spectra were recorded at a resolution of 4 $cm^{-1}$, with an average of 32 scans in transmission mode. Background spectral images were collected under identical conditions from the same $BaF_2$ windows at the beginning and end of each experiment to ensure instrument stability. Water vapor was corrected prior to baseline correction. Post-processing was performed with a lab-made Matlab routine (R2015a, The Mathworks, Natick, CA) and included Mie scattering correction, second derivative spectroscopy and curve fitting routines. Trivalent collagen crosslink content (area ratio 1660 $cm^{-1}$/amide 1), divalent collagen crosslink content (area ratio 1690 $cm^{-1}$/amide 1), total crosslink content (area ratio 1660 + 1690 $cm^{-1}$/amide 1) and collagen maturity (area ratio 1660/1690 $cm^{-1}$) were computed.

### 2.6. Gene expression

For osteoblast cultures, total RNA was extracted after rinsing cultures with PBS. Ex vivo gene expression analysis was performed after crushing left tibia in a mortar with liquid nitrogen. Nucleozol (Macherey-Nagel, Hoerdt, France) was added on top of the cell layer/bone powder and total RNA were purified with Nucleospin RNA set nucleozol column (Macherey-Nagel) according to the manufacturer recommendations. Total RNA was reversed transcribed using iScript cDNA synthesis kit (Bio-Rad) and amplified by real-time PCR using SYBR Green PCR master mix (Bio-Rad). Primer sequences have been entered in Supplementary Table 1. The expression level of each sample was normalized against glyceraldehyde 3-phosphate dehydrogenase (G*apdh*) mRNA expression.

### 2.7. TRAcP staining

Expression of TRAcP was examined cytochemically (Mabilleau et al., 2008). Briefly, cells were rinsed promptly in PBS buffer, fixed with formalin for 10 min and rinsed in distilled water. TRAcP was cytochemically demonstrated by a simultaneous coupling reaction using Naphtol AS-BI-phosphate as substrate and Fast violet B as the diazonium salt. Cells were then incubated for 90 min at 37 °C in the dark, rinsed three times in distilled water and the residual activity was inhibited by 4% NaF for 30 min. Cells were then rinsed in distilled water, counterstained with 4, 6-diamidino-2-phenylindole (DAPI) for 20 min and allowed to dry. TRAcP positive cells, with more than three nuclei, were identified as osteoclasts.

### 2.8. Animals

All procedures were carried out in accordance with the European Union Directive 2010/63/EU for animal experiments and were approved by the regional ethical committee for animal use (authorization CEEA-PdL06-01740.01). Briefly, female BALB/c (BALB/cJRj) mice were obtained from Janvier Labs (Saint-Berthevin, France). Fig. 1 represents the experimental protocols used for this study. Bilateral ovariectomy (OVX) was performed in 24 BALB/c mice at 12 weeks of age under general anesthesia with ketamine (100 mg/kg) and xylazine (10 mg/kg) supplemented with Rimadyl (5 mg/kg). Briefly, mice were lying down on their belly on a warming mat and hairs of the flank area were shaved off. The skin was then disinfected with chlorhexidine solution and lateral incisions of the skin and musculature were performed. The ovarian fat pad was carefully exteriorized from the abdominal cavity, the fallopian tube was cauterized, and the ovaries were dissected. At 16 weeks of age, osmotic minipumps were implanted subcutaneously between the two scapulae in 16 ovariectomized mice that were randomly allocated either into saline daily (OVX + saline, n = 8) or 50 µg/kg/day ($Gly^2$)GLP-2 (OVX + GLP-2, n = 8). ($Gly^2$)GLP-2, also known as Teduglutide, is currently approved for the treatment of short bowel syndrome at this posology (Jeppesen et al., 2011). Eight ovariectomized BALB/c mice received an intravenous injection of zoledronic acid (100 µg/kg) at 16 weeks of age and were used as positive controls (OVX + zoledronic acid). Eight Sham-operated female BALB/c mice with the same age and implanted with osmotic minipumps delivering saline were used as negative controls (Sham + saline). All animals received an intraperitoneal administration of calcein green (10 mg/kg) 10 days and two days before sacrifice. Animals were maintained in a 12 h:12 h light:dark cycle and had free access to water and standard rodent diet (Diet A04, Safe, Augy, France). They were housed 4 animals per cage in the institutional animal laboratory (Agreement E49007002) at 24 °C ± 2 °C. At necropsy, blood collection by intracardiac aspiration (~250 µl) was performed. Blood samples were then spun at 13,000*g* for 15 min, aliquoted and stored at −80 °C. Uterus were collected and weighted to ensure optimum ovariectomy. Right and left tibias, right and left femurs, second (L2) and fourth (L4) lumbar vertebra were collected and cleaned of soft tissue. Right femurs and L2 vertebral bodies were wrapped in saline-soaked gauze and frozen at −20 °C until use. Left tibias were snap frozen in RNAlater and store at −80 °C until use. Other bones were stored in 70% ethanol.

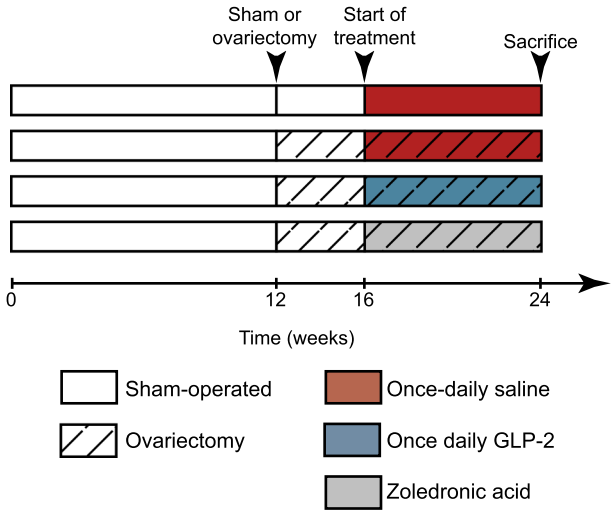


**Fig. 1.** Schematic of the study design.

For two mice in the Sham + saline group and one mouse in the OVX + zoledronic acid group, we did not collect enough blood to store serum. In the OVX + GLP-2 group, one mouse did not recover from the minipump surgery and was euthanized.

### 2.9. ELISA

Serum levels of C-terminal telopeptide of collagen type I (CTx-I) and N-terminal propeptide of type I collagen (P1NP) were measured with the RatLaps CTx-I and Rat/mouse P1NP ELISA kits, respectively (Immunodiagnostic Systems Ltd, Boldon, UK), as recommended by the manufacturer.

### 2.10. High resolution X-ray microcomputed tomography

MicroCT analyses were performed at the right tibia proximal metaphysis with a Skyscan 1272 microtomograph (Bruker-Skyscan, Kontich, Belgium) operated at 70 kV, 140 µA, 1000 ms integration time. The isotropic pixel size was fixed at 4 µm, the rotation step at 0.25° and exposure was performed with a 0.5 mm aluminum filter. The trabecular volume of interest was located 0.5 mm below the growth plate and extended 2 mm down. MicroCT analyses were also performed on left femurs ex vivo with a Skyscan 1076 microtomograph (Bruker-Skyscan) operated at 50 kV, 200 µA, 2000 ms integration time. The isotropic pixel size was fixed at 9 µm, the rotation step at 0.5° and exposure was

performed with a 0.5 mm aluminum filter. The trabecular volume of interest was located 0.5 mm above the growth plate and extended 2 mm up. The cortical volume of interest (1-mm thick) was centered at the midshaft. Analyses of L4 vertebras were done with a Nanotom 180S nanotomograph (GE Phoenix, Solon, Ohio, USA) operated at 85 kV, 220 μA, 1000 ms integration time. The isotropic pixel size was fixed at 4 μm, the rotation step at 0.3° and exposure was performed with a 0.1 mm copper filter. Global thresholding was used for the three investigated bones. All histomorphometrical parameters were measured according to guidelines and nomenclature proposed by the American Society for Bone and Mineral Research (Bouxsein et al., 2010).

### 2.11. Bone histomorphometry

After microCT scans, L4 vertebras were embedded, undecalcified in pMMA at 4 °C to preserve enzyme activities. Bone histomorphometry analysis was restricted only to vertebral bodies as long bones (femur, tibia) were judged too osteopenic (~10% or less in OVX + Veh group) to assess accurately morphometric parameters. This approach has been recommended elsewhere (Recker et al., 2011). For each animal, four non serial longitudinal sections (~50 μm apart) were counterstained with calcein blue for the visualization of mineralized bone structure unstained for the measurement of calcein green-based parameters and four additional sections were stained for the osteoclastic tartrate resistant acid phosphatase (TRAcP), as previously described (Chappard et al., 1983). Histomorphometrical parameters of bone formation have been computed using the CalceinHisto software developed by Professor Rob van't Hof (Institute of Ageing and Chronic Disease – University of Liverpool, UK). Standard bone histomorphometrical nomenclatures, symbol and units were used as described in the guidelines of the American Society for Bone and Mineral Research (Dempster et al., 2013). The identity of the sections was not revealed until the end of all measurements.

### 2.12. Assessment of bone strength

Whole-bone strength of right femurs was assessed by 3-point bending as described previously (Mieczkowska et al., 2013; Ammann et al., 2007) and in accordance with published guidelines (Jepsen et al., 2015). Three-point bending strength was measured with a constant span length of 10 mm. This length is preferred for mouse long bone as it increases the aspect ratio and lead to less error if tissue mechanical properties are computed (Vashishth, 2008). Bones were tested in the antero-posterior axis with the posterior surface facing upward, centered on the support and the pressing force was applied vertically to the midshaft of the bone. Each bone was tested with a loading speed of 2 mm·min$^{-1}$ until failure with a 500 N load cell on an Instron 5942 device (Instron, Elancourt, France) and the load-displacement curve was recorded at a 100 Hz rate by the Bluehill 3 software (Instron). The accuracy of the load cell was guaranteed by the supplier down to 0.5 N. Ultimate load, ultimate displacement, stiffness and work to fracture were calculated as indicated in Turner and Burr (1993). The yield load was calculated with the 0.2% offset method. Post-yield displacement was also computerized. Tissue mechanical properties, computed with Euler-Bernouilli beam theory equations are not totally accurate for mouse long bones (van Lenthe et al., 2008). However, it represents a first approach to evaluate gross differences between controls and treated animals.

Compression test were performed on L2 vertebral bodies with the same device and the load-displacement curve was recorded at a 100 Hz rate with the Bluehill 3 software. Briefly, the caudal surface of the vertebra was glued with cyanoacrylate on the lower platen. A puncture probe (5 mm diameter) was used to apply compression on the cranial surface of the vertebra. Ultimate and yield loads were computed.

### 2.13. Fourier transform infrared imaging (FTIRI)

After microCT, left femurs were embedded undecalcified in pMMA after dehydration and infiltration as previously reported (Mieczkowska et al., 2013). The choice of this resin is preferred for infrared measurements as pMMA does not influence studied parameters (Aparicio et al., 2002). One micrometer-thick section of the midshaft femur were cut with an ultramicrotome (Leica EM UC7, Leica microsystems, Nanterre, France) and deposited on BaF2 windows. Spectral analysis was performed with the same microscope/spectrometer cited above. In order to obtain images, a focal plane array detector (64 × 64 pixels) covering a field of view of 180 × 180 μm was preferred to the standard MCT detector. Cortical bone area at the posterior quadrant covering a field of 540 × 540 μm was examined by FTIRI. Sections were scanned with a spectral resolution of 8 cm$^{-1}$ (spectral region 900–2000 cm$^{-1}$). Each spectrum was corrected for Mie scattering. After pMMA subtraction, spectra were vector normalized for the v1, v3 phosphate band and analyzed with a routine script in Matlab R2015a (The Mathworks, Natick, USA) as previously reported (Aguado et al., 2017). The spectral mineral parameters were: (1) Phosphate/amide ratio (area of v1, v3 phosphate/area amide 1); (2) mineral crystallinity/maturity (intensity ratio 1030 cm$^{-1}$/1020 cm$^{-1}$), reflecting crystal size and perfection; (3) crystal size index (intensity ratio 1075 cm$^{-1}$/1055 cm$^{-1}$), reflecting crystal size in 002, 211, 200 and 202 directions (Gadaleta et al., 1996); (4) acid phosphate content (intensity ratio 1127 cm$^{-1}$/1096 cm$^{-1}$) and (5) carbonate/phosphate ratio (intensity v3 carbonate located at ~1415 cm$^{-1}$/1030 cm$^{-1}$) was computed after subtracting the organic matrix spectrum (Ou-Yang et al., 2001). The spectral organic parameters were: (1) trivalent collagen crosslink content (intensity 1660 cm$^{-1}$/area amide 1) reflecting perturbation exerted on the abundant carbonyl moiety of the collagen molecules by trivalent pyridinoline at ~1660 cm$^{-1}$ (Paschalis et al., 2015); (2) divalent collagen crosslink content (intensity 1690 cm$^{-1}$/area amide 1) reflecting perturbation exerted on the collagen carbonyl by divalent collagen crosslinks at ~1690 cm$^{-1}$ (Paschalis et al., 2001) and (3) collagen maturity (intensity ratio 1660 cm$^{-1}$/1690 cm$^{-1}$) (Paschalis et al., 2001). Histogram distribution for each compositional parameter were fitted with a Gaussian model and considered normally distributed if the $R^2$ coefficient was > 0.95. In the present study, no histogram deviated from normal distribution. For each of the compositional parameters, the mean and full width at half maximum of the pixel distribution (excluding non-bone pixels) were computed and represented as mean and width.

### 2.14. Quantitative backscattered electron imaging (qBEI)

Tissue mineral density was estimated by quantitative backscattered electron imaging as the technical variance is lower than with microCT (Mabilleau et al., 2015). Indeed, the technical variance of our qBEI setup has been estimated at ~0.4%, which is similar to Roschger et al. (1998). qBEI was done on the same blocks and regions as used for FTIRI (Mabilleau et al., 2014). The cortical bone area was imaged at a 200× nominal magnification, corresponding to a pixel size of 0.5 μm per pixel. The region of interest corresponded to the posterior quadrant. The gray levels distribution of each image was analyzed with a lab-made routine using ImageJ. Two variables were obtained from the bone mineral density distribution: $Ca_{mean}$ is the average calcium concentration and $Ca_{width}$ is the width of the histogram at half maximum of the peak.

### 2.15. Statistical analysis

Statistical analyses were performed with GraphPad Prism 6.0 (GraphPad Software, La Jolla, CA, USA). Regarding the small population size in each experiment, normal distribution could not be validated, and non-parametrical statistical test were preferred, as well as

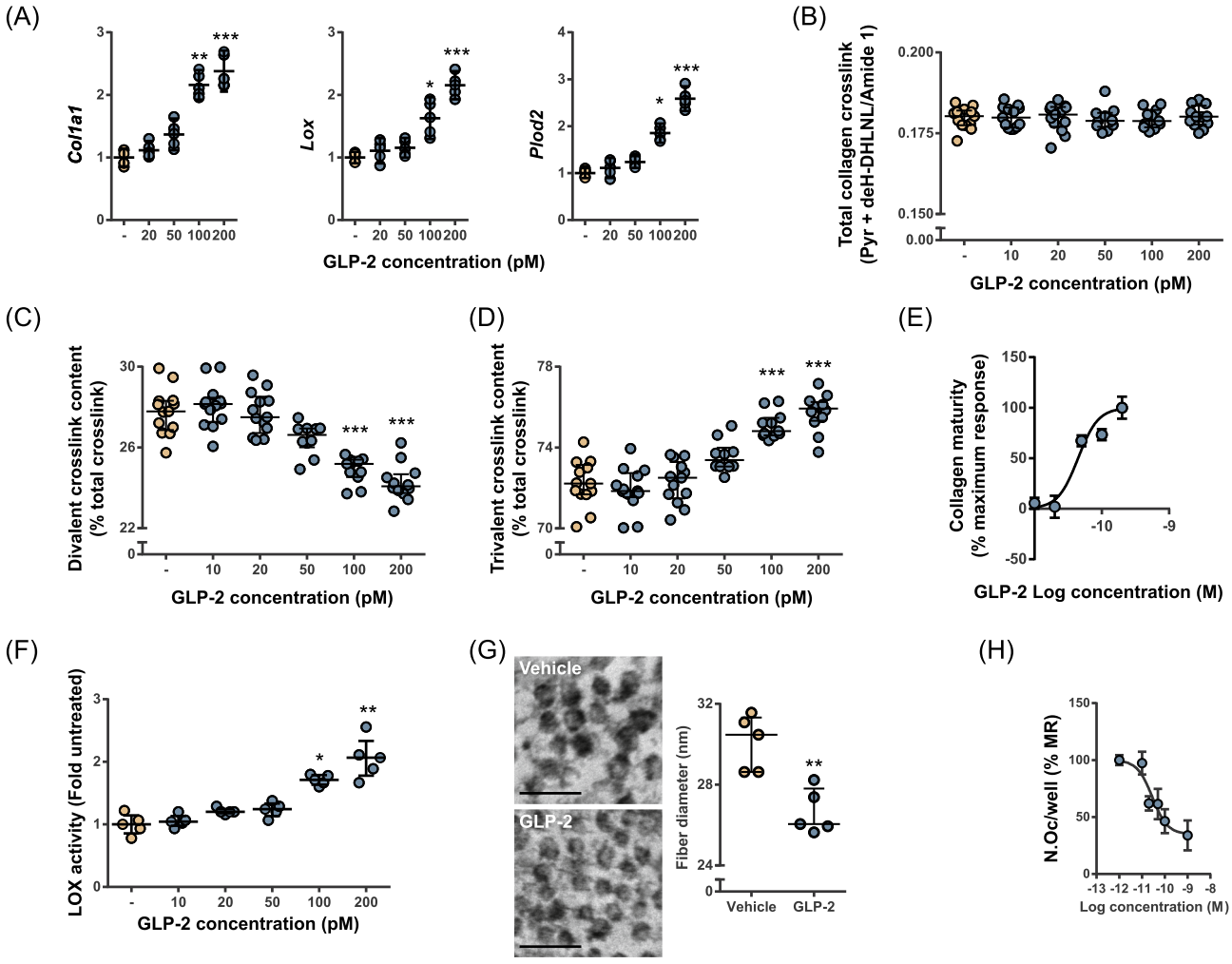


**Fig. 2.** In vitro administration of ($Gly^2$)GLP-2 improves collagen maturity, reduces collagen fiber diameters and inhibits osteoclast differentiation. (A) Effects of ($Gly^2$)GLP-2 administration on osteoblast gene expression. Alpha-1 type I collagen (*Col1a1*), Lysyl hydroxylase 2 (*Plod2*) and lysyl oxidase (*Lox*) expression were evaluated in osteoblast cultures. Total (B), divalent collagen crosslinks (C) and trivalent collagen crosslink content (D) were assessed by Fourier transform infrared microspectroscopy in osteoblast-deposited extracellular matrix. (E) Collagen maturity expressed as the ratio between trivalent and divalent collagen crosslinks was dose-dependently increased in the presence of ($Gly^2$)GLP-2. (F) Lysyl oxidase (LOX) activity was quantified in response to ascending dose of ($Gly^2$)GLP-2. (G) Osteoblast cultures were observed by transmission electron microscopy and collagen fibers with an aspect ratio < 1.2 were measured. Bars = 100 nm. (H) The number of newly generated osteoclasts per well was counted after histochemical detection of the TRAcP enzyme. TRAcP positive cells with more than three nuclei were counted as osteoclasts. Statistical significance was assessed with the non-parametrical Kruskal-Wallis test at the exception of the collagen fiber diameter tested with the Mann-Whitney test. Each experiment has been biologically reproduced between 5 and 15 times independently. Data represent median ± interquartile range. *: $p < 0.05$, **: $p < 0.01$ and ***: $p < 0.001$ vs. vehicle. Orange circles: vehicle, blue circles: ($Gly^2$)GLP-2.

data presentation as scatter plot with median and interquartile range. The Mann-Whitney two-tailed test was used for comparing collagen fiber diameter. All other statistical analyses were done using the Kruskal-Wallis test with Dunn's multiple comparison test. Stepwise multiple linear regressions were performed with Systat 13 software using equation:

Biomechanical investigated properties

$$= f(\beta 0 + \beta 1 \times P1NP + \beta 2 \times Ct.Ar + \beta 3 \times \text{Collagen maturity} + \beta 4 \times \text{Crystal size index} + \beta 5 \times \text{Phosphate/amide})$$

were computerized to evaluate the contribution of each altered biochemical, microarchitectural and compositional parameters on mechanical properties. Differences at $p < 0.05$ were considered significant.

### 2.16. Key resources table

| Resource | Source | Identifier |
|---|---|---|
| *Cell line* | | |
| MC3T3-E1, subclone 4 | ATCC | CRL-2593 |
| Raw 264.7 | ATCC | TIB-7 |
| *Chemical* | | |
| 1,5 diaminopentane | Sigma-Aldrich | C8561 |
| Ascorbic acid | Sigma-Aldrich | A4544 |
| DAPI | Sigma-Aldrich | D9542 |
| EDTA | Sigma-Aldrich | E5134 |
| Fast violet B | Sigma-Aldrich | F1631 |
| Formalin | Merck | 1.00496.5000 |
| Glutaraldehyde | Electron Microscopy Sciences | 16210 |
| Hydrogen peroxide | Sigma-Aldrich | H3410 |
| L-Glutamine | Gibco | 25030-024 |
| Methyl methacrylate | Merck | 8.00590.250 |
| NaF | Sigma-Aldrich | S7920 |
| Naphtol AS-BI-phosphate | Sigma-Aldrich | N2125 |
| Osmium tetroxide | Electron Microscopy Sciences | 19150 |

| | | |
|---|---|---|
| Penicillin/streptomycin | Gibco | 15140-122 |
| Potassium ferricyanide | Electron Microscopy Sciences | 20150 |
| Sodium cacodylate | Electron Microscopy Sciences | 12310 |
| β-Aminopropionitrile | | A13043 |
| Uranyl acetate | Merck | 8473 |
| Urea | Sigma-Aldrich | U0631 |
| Zoledronic acid | Tocris | 6111 |
| *Protein peptide* | | |
| (Gly2)GLP-2 | GeneCust | N/A |
| Horseradish peroxidase | Sigma-Aldrich | P8250 |
| Soluble murine RANKL | Bio-Techne | 462-TEC-010 |
| Type I collagen | Sigma-Aldrich | C3867 |

## 3. Results

### 3.1. (Gly$^2$)GLP-2 affected collagen post-processing, maturity and osteoclastogenesis in vitro

First, we investigated the effects of (Gly$^2$)GLP-2 treatment in MC3T3-E1 cultures. As reported Fig. 2, (Gly$^2$)GLP-2 dose-dependently increased the expression of type 1 collagen, lysyl oxidase and lysyl hydroxylase (Fig. 2A). Although dose-response experiments with ascending concentrations of (Gly$^2$)GLP-2 were undertaken, total collagen crosslink contents, expressed as the sum of trivalent and divalent collagen crosslinks, were not different with increasing GLP-2 concentration (Fig. 2B). However, when trivalent and divalent collagen crosslinks were considered (Fig. 2C–D), (Gly$^2$)GLP-2 was capable of increasing trivalent collagen crosslink content and reducing divalent collagen crosslink content significantly at 100 pM ($p < 0.001$ and $p < 0.001$, respectively) and 200 pM ($p < 0.001$ and $p < 0.001$, respectively). These observations suggested that (Gly$^2$)GLP-2 enhances the maturation of collagen fibers. Indeed, collagen maturity exhibited a sigmoid curve response to ascending concentrations of (Gly$^2$)GLP-2 with an estimated EC50 at 44 ± 5 pM (Fig. 2E). The activity of the lysyl oxidase enzyme, involved in the post-translational maturation of collagen fibers, was also significantly elevated at 100 pM ($p = 0.026$) and 200 pM ($p = 0.002$) (Gly$^2$)GLP-2 (Fig. 2F). Collagen fiber mean diameter was also significantly reduced by 14% ($p = 0.008$) in the presence of 200 pM (Gly$^2$)GLP-2 (Fig. 2G). Taken all together, these data support a direct role of (Gly$^2$)GLP-2 in modifying the collagen matrix.

We also looked at the effect of adding (Gly$^2$)GLP-2 in Raw 264.7 cell cultures. The number of newly generated osteoclasts was significantly and dose-dependently reduced when (Gly$^2$)GLP-2 was added to the cultures with an IC50 estimated at 249 ± 469 pM (Fig. 2H).

### 3.2. (Gly$^2$)GLP-2 did not affect circulating markers of bone remodeling

We next ascertained whether (Gly$^2$)GLP-2, at the approved clinical dose of 50 μg/kg, could improve bone strength and quality in the ovariectomy-induced bone loss and fragility mouse model. We confirmed completeness of ovariectomy by measuring uterus mass at necropsy. Uterus mass was severely reduced in OVX + saline (0.044 ± 0.02 g), OVX + GLP-2 (0.048 ± 0.02 g) and

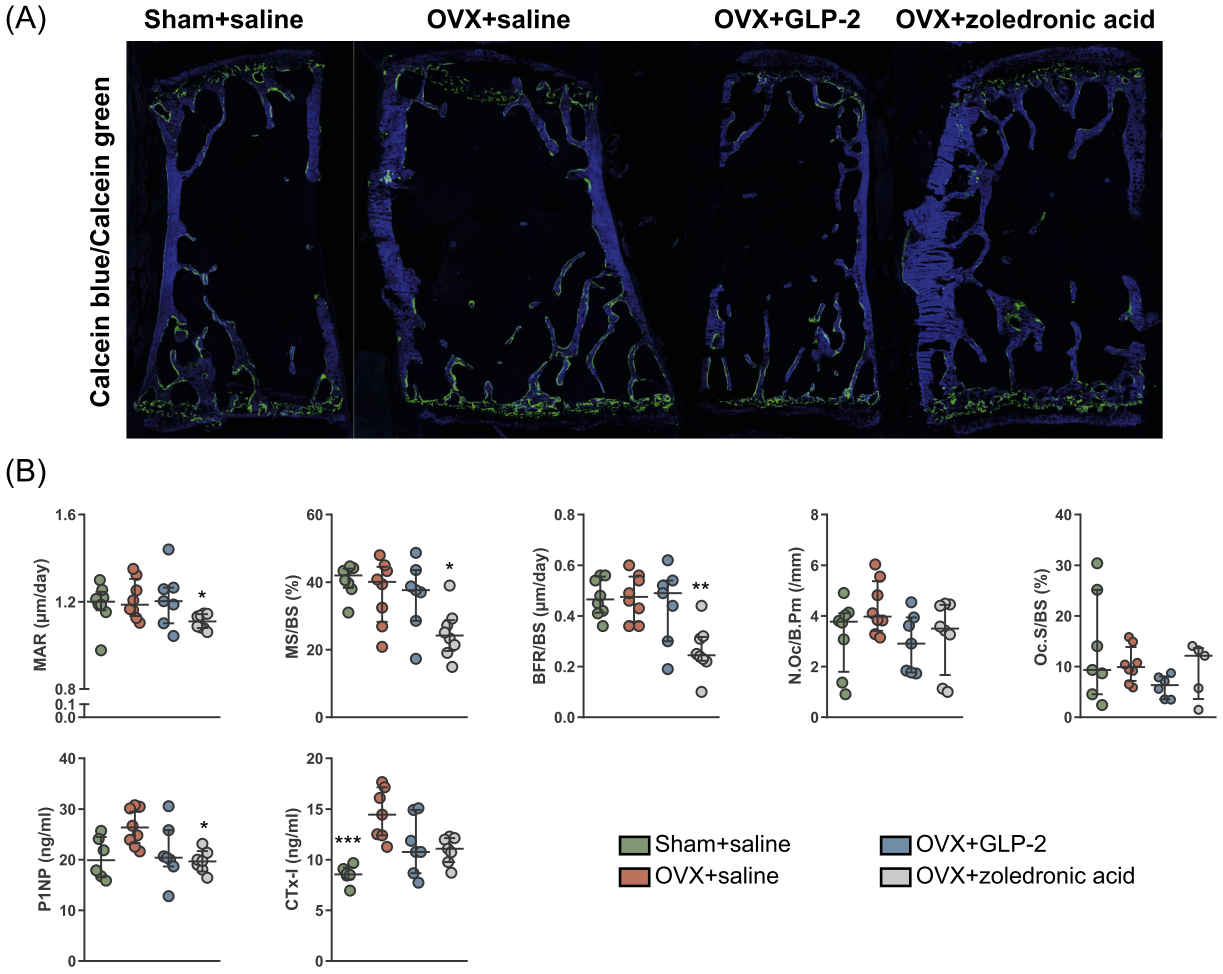


**Fig. 3.** Effects of ovariectomy and (Gly$^2$)GLP-2 or zoledronic intervention on bone histomorphometry. (A) Representative bone sections counterstained with calcein blue. (B) Bone histomorphometry and biochemical parameters. The number of animals per group were n = 6–8. The non-parametrical Kruskal-Wallis test was used and *: $p < 0.05$, **: $p < 0.01$ and ***: $p < 0.001$ vs. OVX + saline group. Data represent median ± interquartile range.

OVX + zoledronic acid (0.038 ± 0.016 g) as compared with Sham animals (0.142 ± 0.035 g) (Supplementary Table 2). We first examined the effects of ovariectomy, but also (Gly$^2$)GLP-2 or zoledronic acid, on bone remodeling. Ovariectomy led to a significant augmentation in circulating CTx levels ($p < 0.001$). However, we did not evidence any significant modifications in MAR, MS/BS, BFR/BS, N.Oc/B.Pm, Oc.S/BS and P1NP in OVX-treated animals (Fig. 3). (Gly$^2$)GLP-2 did not significantly affected any of these histomorphometrical and biochemical parameters. As a positive comparator, zoledronic acid reduced significantly the MAR ($p = 0.046$), MS/BS ($p = 0.046$), BFR/BS ($p = 0.009$) and P1NP levels ($p = 0.014$). CTx-I levels were reduced with zoledronic acid, but unfortunately this reduction did not reach statistical significance ($p = 0.13$).

### 3.3. (Gly$^2$)GLP-2 did not improve bone strength in OVX mice

At the midshaft femur, ovariectomy led to significant alterations of bone strength as represented by reduction in ultimate load (18%, $p < 0.001$), stiffness (31%, $p < 0.001$), yield load (19%, $p < 0.001$) and energy- to-fracture (31%, $p = 0.007$) (Fig. 4A). However, none of GLP-2 or zoledronic acid restored significantly bone strength in OVX mice. Although all the prerequisite for using beam theory equations to estimate tissue-level mechanical properties were not met, we evidenced that ovariectomy led to reductions in elastic modulus (11%, $p = 0.003$) and post-yield strain (34%, $p = 0.037$) (Fig. 4B). Furthermore, GLP-2 and zoledronic acid increased post yield strain significantly (Fig. 4B).

At the L2 lumbar vertebra, OVX did not seem to modify bone strength (Fig. 4C). None of the pharmacological intervention influenced vertebral bone strength.

### 3.4. (Gly$^2$)GLP-2 administration did not restore deteriorated trabecular and cortical bone microarchitectures

Trabecular bone microarchitectures were studied at the L4 vertebral

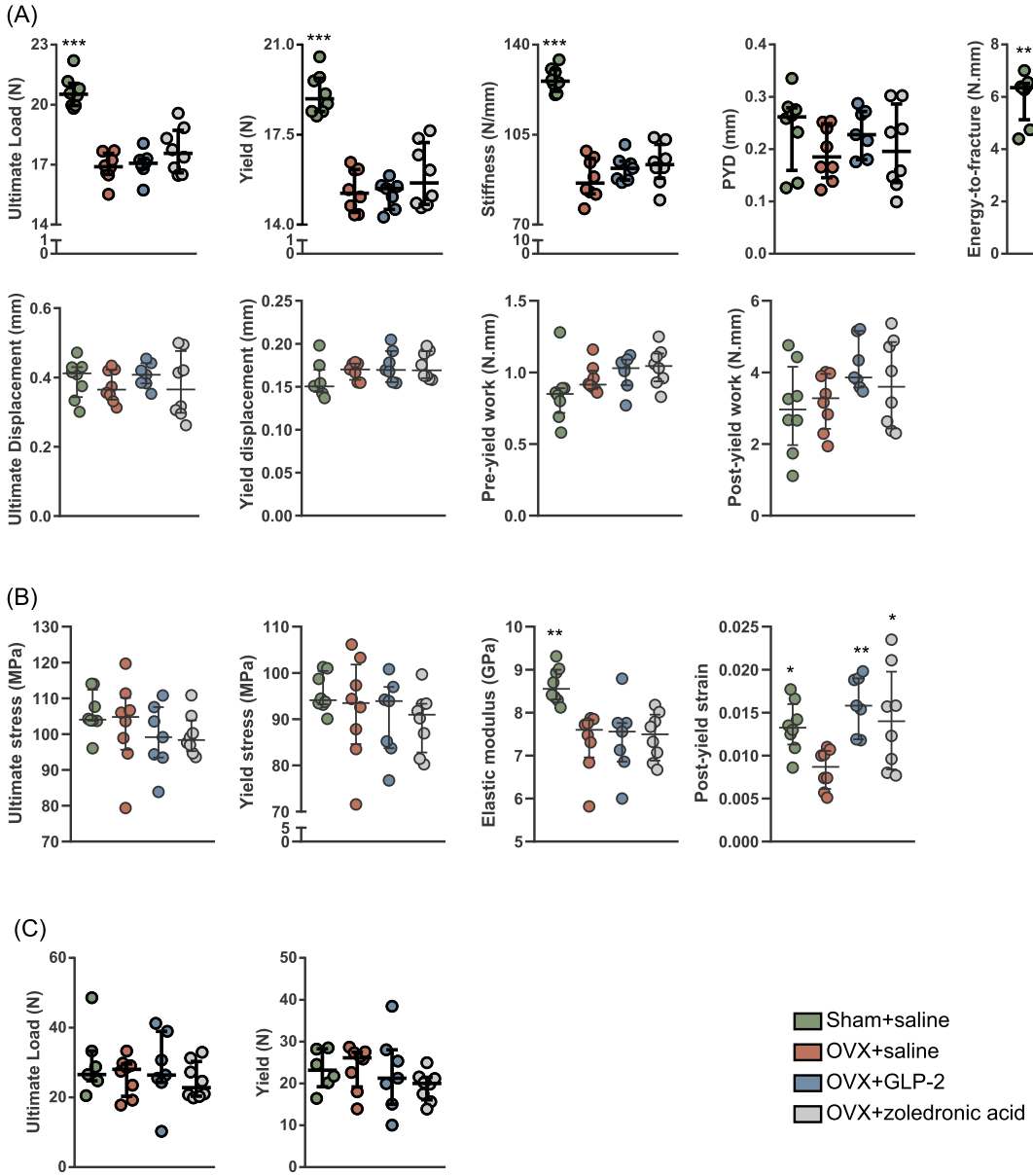


**Fig. 4.** Whole bone mechanical properties from three-point bending and compression test. (A) Whole bone mechanical properties and (B) estimated tissue-level mechanical properties recorded at the femur. (C) Whole bone mechanical properties recorded at the L2 vertebral bodies. PYD: Post-yield displacement. The number of bones tested per group was n = 7–8. The non-parametrical Kruskal-Wallis test was used. **: $p < 0.01$ and ***: $p < 0.001$ vs. OVX + saline group. Data represent median ± interquartile range.

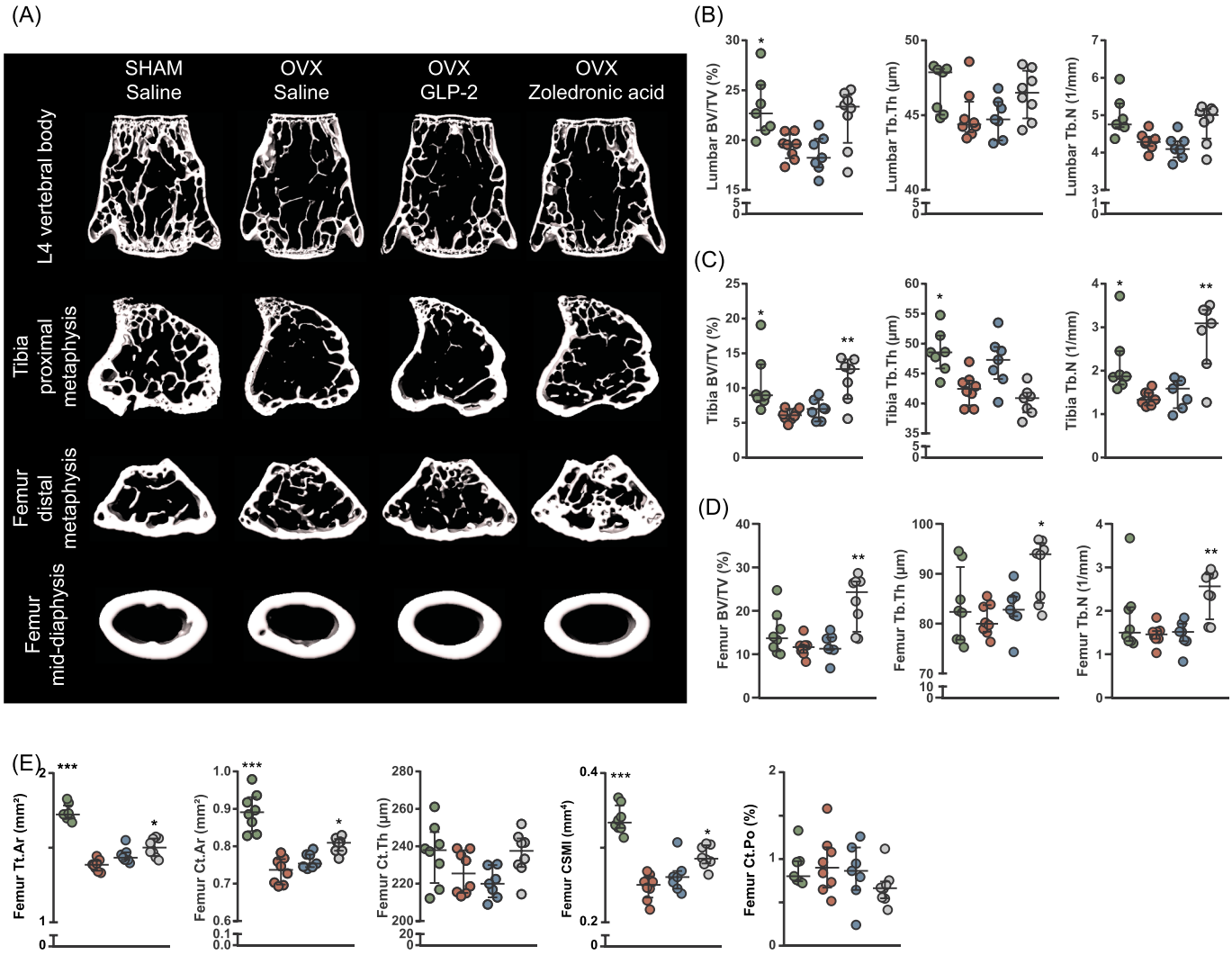


**Fig. 5.** Microarchitectural parameters are affected by ovariectomy but not by ($Gly^2$)GLP-2 treatment. (A) Three-dimensional models of lumbar vertebral bodies, tibia proximal metaphysis, femur distal metaphysis and femur midshaft. Trabecular bone parameters measured in the fourth lumbar vertebral body (B), tibia proximal metaphysis (C) or femur distal metaphysis (D). (E) Cortical bone parameters measured at the femur midshaft. The number of tested bones per group was n = 7–8. The non-parametrical Kruskal-Wallis test was used and *: $p < 0.05$, **: $p < 0.01$ and ***: $p < 0.001$ vs. OVX + saline group. Data represent median ± interquartile range. Green circles: Sham + Saline, red circles: OVX + Saline, blue circles: OVX + GLP-2 and gray circles: OVX + zoledronic acid.

body, tibia proximal metaphysis and distal femoral metaphysis (Fig. 5). In vertebral bodies, a reduction in BV/TV was observed in ovariectomized animals (−14%, p = 0.031). However, although lower values were found for trabecular thickness (p = 0.112) and numbers (p = 0.052), none of these parameters reach statistical significance. ($Gly^2$)GLP-2 and zoledronic acid did not significantly improved vertebral trabecular microarchitecture. At the tibia proximal metaphysis, ovariectomy led to significant reductions in BV/TV (−32%, p = 0.017), Tb.Th (−13%, p = 0.024) and Tb.N (−29%, p = 0.027). Zoledronic acid, but not ($Gly^2$)GLP-2, significantly improved BV/TV (109%, p = 0.008) and Tb.N (132%, p = 0.004). At the femoral distal metaphysis, ovariectomy did not alter significantly either trabecular bone mass or trabecular microarchitecture. At this site, only zoledronic acid, significantly improved BV/TV (93%, p = 0.002), Tb.Th (13%, p = 0.012) and Tb.N (67%, p = 0.008). Cortical bone microarchitecture was studied at the femur midshaft. In our model, ovariectomy led to a significant reduction in cortical area (−17%, $p < 0.001$) but not cortical thickness (p = 0.711). Zoledronic acid, but not ($Gly^2$)GLP-2, resulted in higher Ct.Ar (10%, p = 0.027) but no improvement in cortical thickness (p = 0.483). Taken all together, at trabecular and cortical bone site, ($Gly^2$)GLP-2-treated animals did not present with a bone phenotype significantly different than the one observed in saline-treated ovariectomized mice.

### 3.5. ($Gly^2$)GLP-2 did modify matrix composition in ovariectomized mice

At the tissue level, we first examined the effects of ovariectomy, in our animal model, on collagen properties. As represented Fig. 6, ovariectomy led to significant augmentations of divalent collagen crosslink (5%, p = 0.037) and a non-significant reduction in trivalent collagen crosslink content (p = 0.197). As a consequence, collagen maturity was significantly reduced after ovariectomy by ~8% (p = 0.007). However, when the extent of trivalent and divalent collagen crosslinks were adjusted for the total amount of crosslink, ovariectomy led to a significant accumulation of immature (6%, p = 0.012) and reduction in mature (−2%, p = 0.012) crosslinks (Fig. 6C). On the other hand, ($Gly^2$)GLP-2 and zoledronic acid significantly increased collagen maturity by ~7% (p = 0.018) and ~8% (p = 0.004), respectively (Fig. 6A–B). These

higher collagen maturities were accompanied by non-significant reductions in divalent immature crosslinks and non-significant augmentations in trivalent collagen crosslinks for both molecules (Fig. 6C). At the gene expression level, no changes were observed between the four groups of animals (Fig. 6D).

We next explored whether the mineral compartment of the bone matrix tissue was altered in ovariectomy and how (Gly$^2$)GLP-2 and zoledronic acid could interfere with mineral quality (Fig. 7). Interestingly, ovariectomized mice presented with a significant reduction in crystal size index of ~2% ($p = 0.002$). None of the other parameters were significantly reduced although the phosphate/amide ratio was close to significance ($p = 0.058$). (Gly$^2$)GLP-2 significantly reduced the phosphate/amide ratio by ~2% ($p = 0.019$) and led to higher heterogeneity of acid phosphate distribution (20%, $p = 0.003$) within the bone matrix. On the other hand, at the exception of higher heterogeneity in crystallinity distribution (25%, $p = 0.006$), zoledronic acid did not change mineral quality properties. qBEI analyses failed to highlight any significant difference in absolute mineral content accumulation in the bone matrix.

### 3.6. Bone fragility in ovariectomized mice is associated with cortical area, mineral crystal size and maturity of the collagen matrix

In order to ascertain which of the altered parameters (biochemical, microarchitectural and/or compositional) were important for reduced bone strength in ovariectomized mice, we performed stepwise multiple linear regression analyses. As reported in Table 1, ultimate and yield load were only correlated with the microarchitectural parameter Ct.Ar. On the other hand, stiffness of the cortical bone matrix was significantly and positively associated with Ct.Ar but also crystal size index. The energy-to-fracture, representing the work that must be done to fracture bone, was associated with the compositional parameters crystal size index and collagen maturity.

## 4. Discussion

Osteoporosis is a chronic bone disease characterized by low bone mass and deterioration of bone tissue at all scales that contributes to lower bone quality and strength, and ultimately to an increased risk of

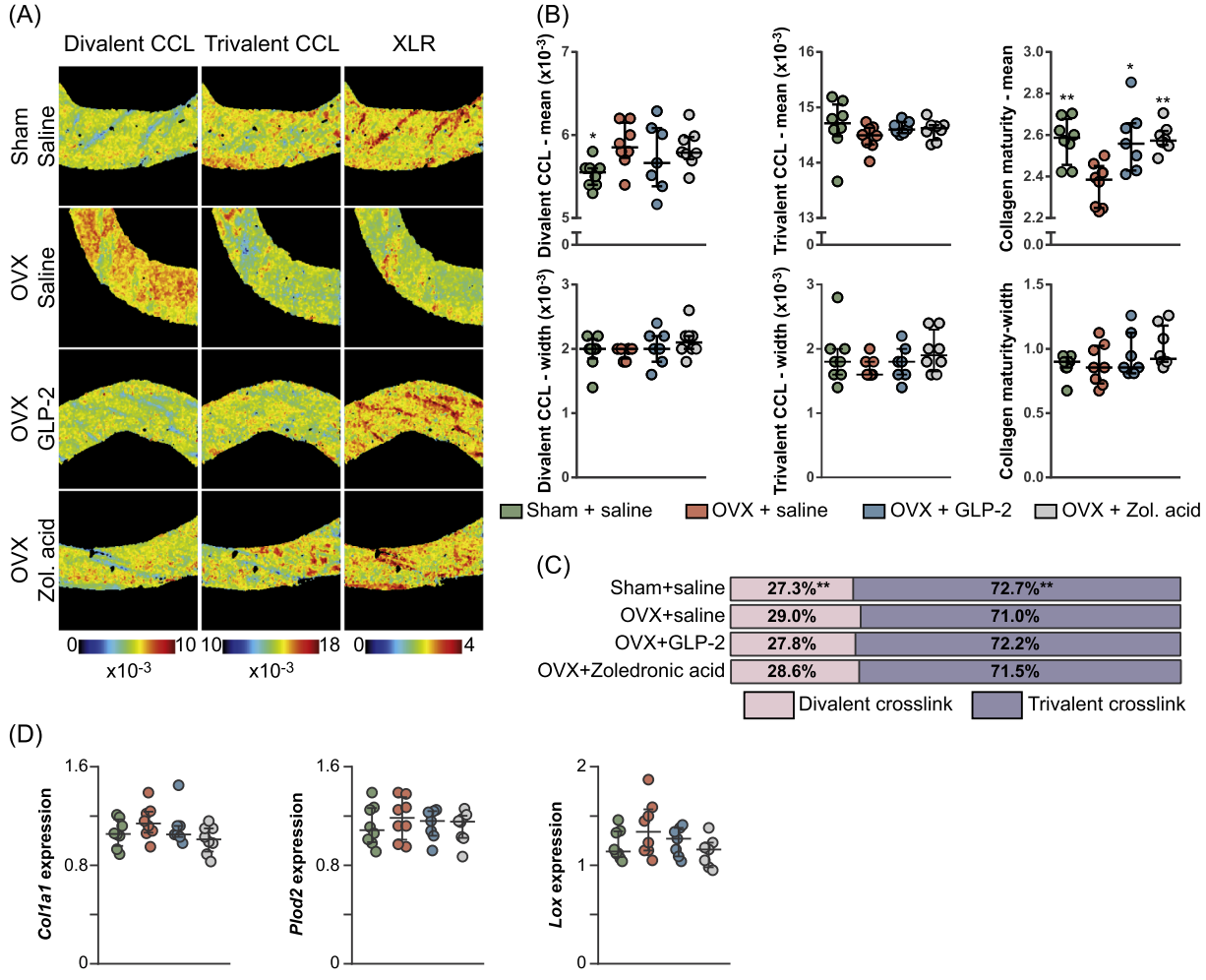


**Fig. 6.** (Gly$^2$)GLP-2 increased collagen maturity. Collagen properties were assessed by Fourier transform infrared imaging (FTIRI) as divalent collagen crosslink (Divalent CCL), trivalent collagen crosslink content (Trivalent CCL) and collagen maturity (XLR). (A) Representative infrared images and (B) corresponding mean and width for divalent collagen crosslink content, trivalent collagen crosslink content and collagen maturity. (C) The extent of divalent collagen crosslink and trivalent collagen crosslink content were adjusted for total collagen crosslinks. (D) Gene expression of alpha-1 type I collagen (*Col1a1*), lysyl hydroxylase 2 (*Plod2*) and lysyl oxidase (*Lox*) measured at the tibia. The number of tested bones per group was n = 7–8. The non-parametrical Kruskal-Wallis test was used and *: $p < 0.05$ and **: $p < 0.01$ vs. OVX + saline group. Data represent median ± interquartile range.

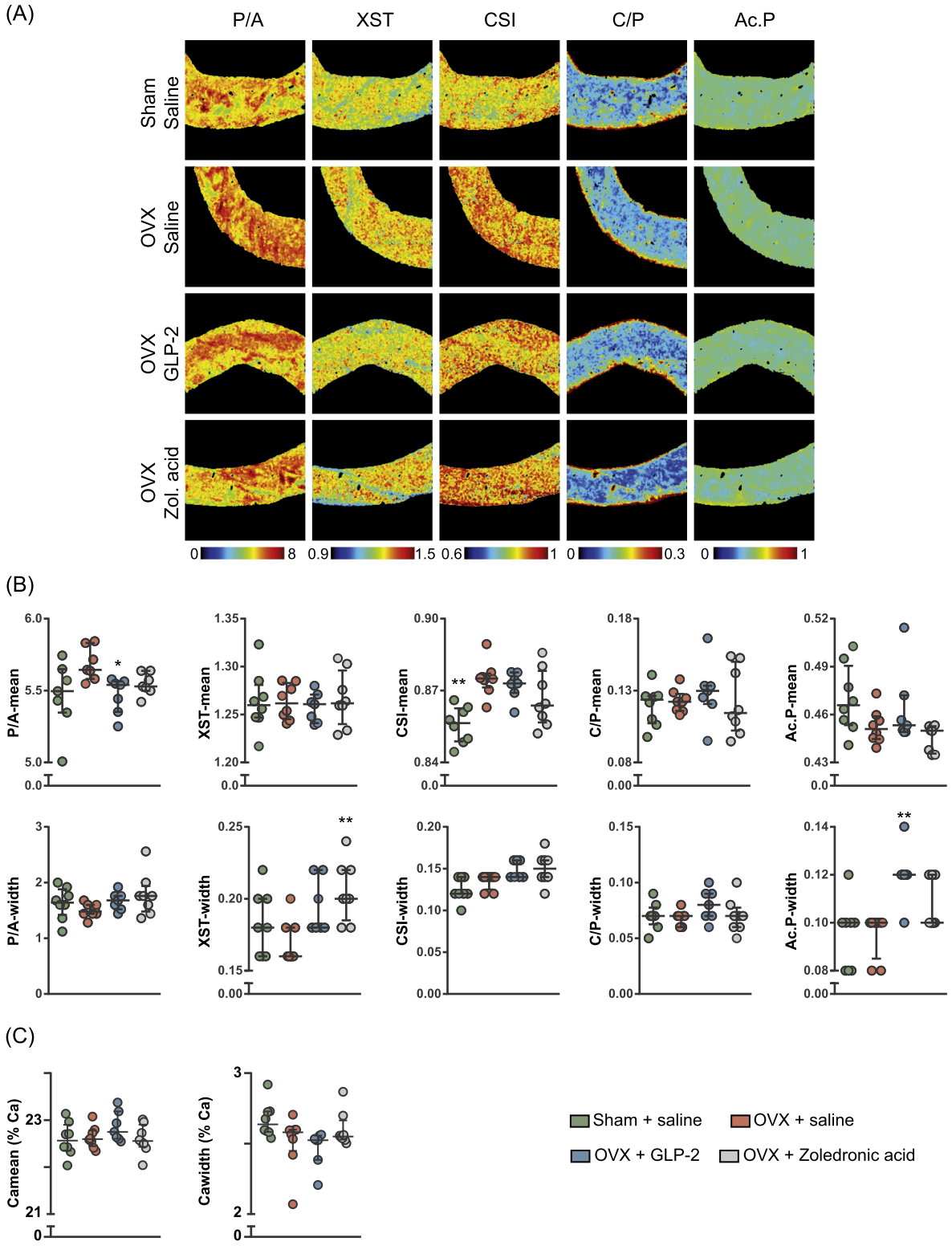


**Fig. 7.** Effects of (Gly$^2$)GLP-2 administration on bone mineral properties. (A) Representative infrared images of phosphate/amide (P/A), mineral crystallinity (XST), crystal size index (CSI), carbonate/phosphate ratio (C/P) and acid phosphate content. (B) Mean and width of each mineral parameters determined by infrared imaging. (C) Calcium content (Camean) and heterogeneity (Cawidth) determined by quantitative backscattered electron imaging. The number of tested bones per group was n = 7–8. The non-parametrical Kruskal-Wallis test was used and *: $p < 0.05$ and **: $p < 0.01$ vs. OVX + saline group. Data represent median ± interquartile range.

bone fracture. Alteration of bone remodeling contributes to lower bone mass and modifications of bone microstructure. Furthermore, by altering the maturation kinetic of the bone matrix, bone remodeling contributes also to modifications of bone tissue component independently of a direct action on biomolecules synthesis and secretion by bone cells. Previous biochemical assessment of circulating bone turnover markers suggested a circadian pattern, with reduced bone resorption during daytime followed by a nocturnal increase (Aoshima

**Table 1**
Stepwise multiple linear regression between biomechanical, biochemical, microarchitectural and compositional bone parameters.

| Dependent variable | Model adjusted $R^2$ | Model p value | Parameter | β | Parameter p value |
|---|---|---|---|---|---|
| Ultimate load | 0.83 | < 0.001 | Ct.Ar | 16.2 | < 0.001 |
| Yield load | 0.88 | < 0.001 | Ct.Ar | 17.4 | < 0.001 |
| Stiffness | 0.83 | < 0.001 | Intercept | 521.6 | 0.047 |
| | | | Ct.Ar | 144.7 | 0.001 |
| | | | Crystal size index | −615.0 | 0.030 |
| Energy-to-fracture | 0.68 | < 0.001 | Intercept | 37.0 | 0.045 |
| | | | Collagen maturity | 4.0 | 0.012 |
| | | | Crystal size index | −48.3 | 0.014 |

et al., 1998; Schlemmer et al., 1994; Wichers et al., 1999). Several studies have attempted to identify the factors associated with this circadian pattern and showed that this diurnal variation is independent of age, menopausal status, serum cortisol, serum PTH and serum melatonin (Aoshima et al., 1998; Schlemmer et al., 1994; Heshmati et al., 1998; Ledger et al., 1995; Ostrowska et al., 2001). Interestingly, the circadian variation of bone resorption is dampened significantly in fasting individuals (Schlemmer and Hassager, 1999). As such it has been postulated that the nocturnal rise in bone resorption could represent a consequence of the insufficient access to nutrients and minerals to maintain plasma calcium homeostasis. An interest for the secretion products of enteroendocrine cells, that sense nutrients and minerals entry into the intestine lumen, has then emerged. Among intestinal hormones, an interest for GLP-2 has been raised on the basis that a single subcutaneous administration of GLP-2 was capable of reducing circulating bone turnover marker of bone resorption (Henriksen et al., 2003). As now some GLP-2 analogues have been developed with a longer plasma half-life, we thought to investigate whether GLP-2 analogues could represent alternative medications in the treatment of bone fragility. In the present study, we demonstrated undoubtedly that, in vitro, ($Gly^2$)GLP-2 was acting on osteoblast cells directly and stimulated the expression of factors involved either in the bone matrix deposition or maturation. Furthermore, we showed a direct action of ($Gly^2$)GLP-2 in enhancing maturation of the collagen matrix and a direct action in vitro in reducing the differentiation of osteoclast precursors into mature osteoclasts. However, the administration of ($Gly^2$)GLP-2, at the clinical dose of 50 μg/kg in ovariectomized Balb/c mice, resulted in disappointing results with no improvement in whole-bone strength or microstructure, and only modest ameliorations in collagen maturity and phosphate/amide ratio of the bone matrix. The latter was not mirrored in qBEI data suggesting that modulation of phosphate/amide ratio observed in the presence of ($Gly^2$)-GLP-2 may be due to changes in collagen quantity rather than mineral accumulation. However, this was not confirmed by gene expression analysis and further studies will be required to fully understand this phenotype.

The current observation contrast with those of Xu et al. who showed positive effects of GLP-2 administration in ovariectomized rats (Xu et al., 2019). They found that GLP-2 enhanced osteoblast activity with higher level of ALP activity and P1NP compared to saline-injected rats. Microarchitecture analysis in this specific study revealed that GLP-2 increased significantly bone trabecular volume and trabecular number compared to saline-injected rats. However, several differences in the experimental model used by Xu et al. and ours have been noticed. Firstly, Xu et al. started GLP-2 administration 3 months post-ovariectomy in ~38–40-week-old rats whereas in our study GLP-2 administration was initiated 4 week post-surgery in 16 week-old mice. Secondly, the dose of GLP-2 used in Xu et al. was 3 times higher than in our study. Henriksen and Holst, also reported positive effects of ($Gly^2$)GLP-2 in preserving bone mass density in ovariectomized aged rats but at a dose 5 times higher than used in our study (Henriksen and Holst, 2008). The pharmacokinetic profile of ($Gly^2$)GLP-2 has been extensively studied and the plasmatic concentration reached after a subcutaneous injection of 50 μg/kg is around ~7–10 nmol/^l (Marier et al., 2010). Based on the concentrations and $EC_{50}$/$IC_{50}$ observed in the present study for action on collagen maturity and osteoclast differentiation, the dose of 50 μg/kg seemed adequate. However, it is plausible that the dose of 50 μg/kg used in our study was not enough high to exhibit positive actions on bone strength and microstructure in a rodent model of bone fragility.

Another plausible scenario resides in the mode of administration. In the study of Xu et al., and Henriksen and Holst, administration was performed by daily subcutaneous administration (Xu et al., 2019; Henriksen and Holst, 2008). In the present study, we chose to administer ($Gly^2$)GLP-2 with minipumps, delivering a constant flow rate of ~1 ng/min (equivalent to ~0.3 pmol/min). Previous published studies reported a rapid desensitization of the GLP-2 receptor, at dose in the nmol range, involving unique signaling pathways that were lipid raft dependent but clathrin-, dynamin-, and β-arrestin independent (Estall et al., 2005; Estall et al., 2004). However, it is plausible that the long-term stimulation with low dose, as conducted to the present study, led to a significant reduction in response or desensitization of the GLP-2 receptor. Further studies are required to fully appreciate the pharmacology of the GLP-2 receptor in order to identify the best regimen of administration.

Nevertheless, ($Gly^2$)GLP-2 was capable of enhancing the collagen maturity in vitro but also in vivo confirming osteoblasts as a target of GLP-2, at least in rodent. This is further confirmed by the bone phenotype observed in GLP-2 receptor knock out animals where a decreased osteoblast activity was observed (Undale et al., 2006). However, GLP-2r KO mice at 6 weeks of age exhibited also a significant reduction in bone mass and density suggesting a strong role of GLP-2 receptor signaling in controlling bone development and physiology. These results may seem discordant from ours, but it is important to bear in mind that in our study, exogenous administration of GLP-2, although targeting the GLP-2/GLP-2r pathway, may be quite different in response than deleting the receptor. On the other hand, our in vitro results are similar to the published results. We demonstrate in our study that GLP-2 decreased osteoclast formation from Raw 264.7 cells. One previous study found that Raw 264.7 infected with lentivirus rLV-Green-GLP2 had a significant decreased TRAP activity at the fourth and fifth day of differentiation. The formation rate of osteoclast was also significantly decreased in rLV-Green-GLP2 group (Lu et al., 2018).

In conclusion, our study highlighted that in the ovariectomy-induced bone loss mouse model, the administration of 50 μg/kg ($Gly^2$)GLP-2 for 8 weeks was not enough to improve bone mass, microarchitecture, quality and more importantly strength. Further studies with different dose and regimen of administration are required to appreciate whether ($Gly^2$)GLP-2 might be beneficial in humans suffering of bone fragility.

Supplementary data to this article can be found online at https://doi.org/10.1016/j.bonr.2020.100251.

## Transparency document

The Transparency document associated this article can be found, in online version.

## Declaration of competing interest

None of the authors have any conflict of interest to report.

## Acknowledgements

The authors are grateful to Nadine Gaborit and Stéphanie Lemière (University of Angers, GEROM-LHEA, Institut de Biologie en Santé, Angers, France) for their help with microCT. We are thankful to Prof Peter Gardner (University of Manchester) for supplying the Mie scattering correction routine for Matlab and Prof Rob van't Hof for supplying the CalceinHisto software. Part of this work was supported by a grant from the SATT Ouest valorization (grant number DV2541).

## References

Aguado, E., Mabilleau, G., Goyenvalle, E., Chappard, D., 2017. Hypodynamia alters bone quality and trabecular microarchitecture. Calcif. Tissue Int. 100 (4), 332–340.
Ammann, P., Badoud, I., Barraud, S., Dayer, R., Rizzoli, R., 2007. Strontium ranelate treatment improves trabecular and cortical intrinsic bone tissue quality, a determinant of bone strength. J. Bone Miner. Res. 22 (9), 1419–1425.
Aoshima, H., Kushida, K., Takahashi, M., Ohishi, T., Hoshino, H., Suzuki, M., Inoue, T., 1998. Circadian variation of urinary type I collagen crosslinked C-telopeptide and free and peptide-bound forms of pyridinium crosslinks. Bone 22 (1), 73–78.
Aparicio, S., Doty, S.B., Camacho, N.P., Paschalis, E.P., Spevak, L., Mendelsohn, R., Boskey, A.L., 2002. Optimal methods for processing mineralized tissues for Fourier transform infrared microspectroscopy. Calcif. Tissue Int. 70 (5), 422–429.
Bedell-Hogan, D., Trackman, P., Abrams, W., Rosenbloom, J., Kagan, H., 1993. Oxidation, cross-linking, and insolubilization of recombinant tropoelastin by purified lysyl oxidase. J. Biol. Chem. 268 (14), 10345–10350.
Boskey, A.L., 2013. Bone composition: relationship to bone fragility and antiosteoporotic drug effects. BoneKEy Rep. 2, 447.
Bouxsein, M.L., Boyd, S.K., Christiansen, B.A., Guldberg, R.E., Jepsen, K.J., Muller, R., 2010. Guidelines for assessment of bone microstructure in rodents using micro-computed tomography. J. Bone Miner. Res. 25 (7), 1468–1486.
Brubaker, P.L., 2018. Glucagon-like peptide-2 and the regulation of intestinal growth and function. Compr. Physiol. 8 (3), 1185–1210.
Chappard, D., Alexandre, C., Riffat, G., 1983. Histochemical identification of osteoclasts. Review of current methods and reappraisal of a simple procedure for routine diagnosis on undecalcified human iliac bone biopsies. Basic Appl. Histochem. 27 (2), 75–85.
Chappard, D., Basle, M.F., Legrand, E., Audran, M., 2011. New laboratory tools in the assessment of bone quality. Osteoporos. Int. 22 (8), 2225–2240.
Consensus development conference: diagnosis, prophylaxis, and treatment of osteoporosis. Am. J. Med. 94 (6), 646–650.
Cummings, S.R., San Martin, J., McClung, M.R., Siris, E.S., Eastell, R., Reid, I.R., Delmas, P., Zoog, H.B., Austin, M., Wang, A., Kutilek, S., Adami, S., Zanchetta, J., Libanati, C., Siddhanti, S., Christiansen, C., Trial, F., 2009. Denosumab for prevention of fractures in postmenopausal women with osteoporosis. N. Engl. J. Med. 361 (8), 756–765.
Dempster, D.W., Compston, J.E., Drezner, M.K., Glorieux, F.H., Kanis, J.A., Malluche, H., Meunier, P.J., Ott, S.M., Recker, R.R., Parfitt, A.M., 2013. Standardized nomenclature, symbols, and units for bone histomorphometry: a 2012 update of the report of the ASBMR Histomorphometry Nomenclature Committee. J. Bone Miner. Res. 28 (1), 2–17.
Drucker, D.J., Habener, J.F., Holst, J.J., 2017. Discovery, characterization, and clinical development of the glucagon-like peptides. J. Clin. Invest. 127 (12), 4217–4227.
Estall, J.L., Yusta, B., Drucker, D.J., 2004. Lipid raft-dependent glucagon-like peptide-2 receptor trafficking occurs independently of agonist-induced desensitization. Mol. Biol. Cell 15 (8), 3673–3687.
Estall, J.L., Koehler, J.A., Yusta, B., Drucker, D.J., 2005. The glucagon-like peptide-2 receptor C terminus modulates beta-arrestin-2 association but is dispensable for ligand-induced desensitization, endocytosis, and G-protein-dependent effector activation. J. Biol. Chem. 280 (23), 22124–22134.
Ettinger, B., Black, D.M., Mitlak, B.H., Knickerbocker, R.K., Nickelsen, T., Genant, H.K., Christiansen, C., Delmas, P.D., Zanchetta, J.R., Stakkestad, J., Gluer, C.C., Krueger, K., Cohen, F.J., Eckert, S., Ensrud, K.E., Avioli, L.V., Lips, P., Cummings, S.R., 1999. Reduction of vertebral fracture risk in postmenopausal women with osteoporosis treated with raloxifene: results from a 3-year randomized clinical trial. Multiple Outcomes of Raloxifene Evaluation (MORE) Investigators. Jama 282 (7), 637–645.
Gadaleta, S.J., Paschalis, E.P., Betts, F., Mendelsohn, R., Boskey, A.L., 1996. Fourier transform infrared spectroscopy of the solution-mediated conversion of amorphous calcium phosphate to hydroxyapatite: new correlations between X-ray diffraction and infrared data. Calcif. Tissue Int. 58 (1), 9–16.
Gaudin-Audrain, C., Irwin, N., Mansur, S., Flatt, P.R., Thorens, B., Basle, M., Chappard, D., Mabilleau, G., 2013. Glucose-dependent insulinotropic polypeptide receptor deficiency leads to modifications of trabecular bone volume and quality in mice. Bone 53 (1), 221–230.
Hartmann, B., Harr, M.B., Jeppesen, P.B., Wojdemann, M., Deacon, C.F., Mortensen, P.B., Holst, J.J., 2000. In vivo and in vitro degradation of glucagon-like peptide-2 in humans. J. Clin. Endocrinol. Metab. 85 (8), 2884–2888.
D.B. Henriksen, J.J. Holst, Use of GLP-2 and related compounds for the treatment, prevention, diagnosis, and prognosis of bone-related disroders and calcium homeostasis related syndromes, US 7,371,721 B2, 2008.
Henriksen, D.B., Alexandersen, P., Bjarnason, N.H., Vilsboll, T., Hartmann, B., Henriksen, E.E., Byrjalsen, I., Krarup, T., Holst, J.J., Christiansen, C., 2003. Role of gastrointestinal hormones in postprandial reduction of bone resorption. J. Bone Miner. Res. 18 (12), 2180–2189.
Henriksen, D.B., Alexandersen, P., Byrjalsen, I., Hartmann, B., Bone, H.G., Christiansen, C., Holst, J.J., 2004. Reduction of nocturnal rise in bone resorption by subcutaneous GLP-2. Bone 34 (1), 140–147.
Henriksen, D.B., Alexandersen, P., Hartmann, B., Adrian, C.L., Byrjalsen, I., Bone, H.G., Holst, J.J., Christiansen, C., 2007. Disassociation of bone resorption and formation by GLP-2: a 14-day study in healthy postmenopausal women. Bone 40 (3), 723–729.
Henriksen, D.B., Alexandersen, P., Hartmann, B., Adrian, C.L., Byrjalsen, I., Bone, H.G., Holst, J.J., Christiansen, C., 2009. Four-month treatment with GLP-2 significantly increases hip BMD: a randomized, placebo-controlled, dose-ranging study in postmenopausal women with low BMD. Bone 45 (5), 833–842.
Heshmati, H.M., Riggs, B.L., Burritt, M.F., McAlister, C.A., Wollan, P.C., Khosla, S., 1998. Effects of the circadian variation in serum cortisol on markers of bone turnover and calcium homeostasis in normal postmenopausal women. J. Clin. Endocrinol. Metab. 83 (3), 751–756.
Jeppesen, P.B., Gilroy, R., Pertkiewicz, M., Allard, J.P., Messing, B., O'Keefe, S.J., 2011. Randomised placebo-controlled trial of teduglutide in reducing parenteral nutrition and/or intravenous fluid requirements in patients with short bowel syndrome. Gut 60 (7), 902–914.
Jepsen, K.J., Silva, M.J., Vashishth, D., Guo, X.E., van der Meulen, M.C., 2015. Establishing biomechanical mechanisms in mouse models: practical guidelines for systematically evaluating phenotypic changes in the diaphyses of long bones. J. Bone Miner. Res. 30 (6), 951–966.
Khosla, S., Bilezikian, J.P., Dempster, D.W., Lewiecki, E.M., Miller, P.D., Neer, R.M., Recker, R.R., Shane, E., Shoback, D., Potts, J.T., 2012. Benefits and risks of bisphosphonate therapy for osteoporosis. J. Clin. Endocrinol. Metab. 97 (7), 2272–2282.
Ledger, G.A., Burritt, M.F., Kao, P.C., O'Fallon, W.M., Riggs, B.L., Khosla, S., 1995. Role of parathyroid hormone in mediating nocturnal and age-related increases in bone resorption. J. Clin. Endocrinol. Metab. 80 (11), 3304–3310.
van Lenthe, G.H., Voide, R., Boyd, S.K., Muller, R., 2008. Tissue modulus calculated from beam theory is biased by bone size and geometry: implications for the use of three-point bending tests to determine bone tissue modulus. Bone 43 (4), 717–723.
Lu, Y., Lu, D., Hu, Y., 2018. Glucagon-like peptide 2 decreases osteoclasts by stimulating apoptosis dependent on nitric oxide synthase. Cell Prolif. 51 (4), e12443.
Mabilleau, G., 2017. Interplay between bone and incretin hormones: a review. Morphologie 101 (332), 9–18.
Mabilleau, G., Petrova, N.L., Edmonds, M.E., Sabokbar, A., 2008. Increased osteoclastic activity in acute Charcot's osteoarthropathy: the role of receptor activator of nuclear factor-kappaB ligand. Diabetologia 51 (6), 1035–1040.
Mabilleau, G., Mieczkowska, A., Irwin, N., Flatt, P.R., Chappard, D., 2013. Optimal bone mechanical and material properties require a functional glucagon-like peptide-1 receptor. J. Endocrinol. 219 (1), 59–68.
Mabilleau, G., Mieczkowska, A., Irwin, N., Simon, Y., Audran, M., Flatt, P.R., Chappard, D., 2014. Beneficial effects of a N-terminally modified GIP agonist on tissue-level bone material properties. Bone 63, 61–68.
Mabilleau, G., Mieczkowska, A., Libouban, H., Simon, Y., Audran, M., Chappard, D., 2015. Comparison between quantitative X-ray imaging, dual energy X-ray absorptiometry and microCT in the assessment of bone mineral density in disuse-induced bone loss. J. Musculoskelet. Neuronal Interact. 15 (1), 42–52.
Marier, J.F., Mouksassi, M.S., Gosselin, N.H., Beliveau, M., Cyran, J., Wallens, J., 2010. Population pharmacokinetics of teduglutide following repeated subcutaneous administrations in healthy participants and in patients with short bowel syndrome and Crohn's disease. J. Clin. Pharmacol. 50 (1), 36–49.
McClung, M., Harris, S.T., Miller, P.D., Bauer, D.C., Davison, K.S., Dian, L., Hanley, D.A., Kendler, D.L., Yuen, C.K., Lewiecki, E.M., 2013. Bisphosphonate therapy for osteoporosis: benefits, risks, and drug holiday. Am. J. Med. 126 (1), 13–20.
Mieczkowska, A., Irwin, N., Flatt, P.R., Chappard, D., Mabilleau, G., 2013. Glucose-dependent insulinotropic polypeptide (GIP) receptor deletion leads to reduced bone strength and quality. Bone 56 (2), 337–342.
Mieczkowska, A., Bouvard, B., Chappard, D., Mabilleau, G., 2015. Glucose-dependent insulinotropic polypeptide (GIP) directly affects collagen fibril diameter and collagen cross-linking in osteoblast cultures. Bone 74, 29–36.
Neer, R.M., Arnaud, C.D., Zanchetta, J.R., Prince, R., Gaich, G.A., Reginster, J.Y., Hodsman, A.B., Eriksen, E.F., Ish-Shalom, S., Genant, H.K., Wang, O., Mitlak, B.H., 2001. Effect of parathyroid hormone (1–34) on fractures and bone mineral density in postmenopausal women with osteoporosis. N. Engl. J. Med. 344 (19), 1434–1441.
Ostrowska, Z., Kos-Kudla, B., Marek, B., Swietochowska, E., Gorski, J., 2001. Assessment of the relationship between circadian variations of salivary melatonin levels and type I collagen metabolism in postmenopausal obese women. Neuro Endocrinol. Lett. 22 (2), 121–127.
Ou-Yang, H., Paschalis, E.P., Mayo, W.E., Boskey, A.L., Mendelsohn, R., 2001. Infrared microscopic imaging of bone: spatial distribution of CO3(2-). J. Bone Miner. Res. 16 (5), 893–900.
Paschalis, E.P., Verdelis, K., Doty, S.B., Boskey, A.L., Mendelsohn, R., Yamauchi, M., 2001. Spectroscopic characterization of collagen cross-links in bone. J. Bone Miner. Res. 16 (10), 1821–1828.
Paschalis, E.P., Gamsjaeger, S., Tatakis, D.N., Hassler, N., Robins, S.P., Klaushofer, K., 2015. Fourier transform infrared spectroscopic characterization of mineralizing type I collagen enzymatic trivalent cross-links. Calcif. Tissue Int. 96 (1), 18–29.
Recker, R.R., Kimmel, D.B., Dempster, D., Weinstein, R.S., Wronski, T.J., Burr, D.B., 2011. Issues in modern bone histomorphometry. Bone 49 (5), 955–964.

Roschger, P., Fratzl, P., Eschberger, J., Klaushofer, K., 1998. Validation of quantitative backscattered electron imaging for the measurement of mineral density distribution in human bone biopsies. Bone 23 (4), 319–326.
Schlemmer, A., Hassager, C., 1999. Acute fasting diminishes the circadian rhythm of biochemical markers of bone resorption. Eur. J. Endocrinol. 140 (4), 332–337.
Schlemmer, A., Hassager, C., Pedersen, B.J., Christiansen, C., 1994. Posture, age, menopause, and osteopenia do not influence the circadian variation in the urinary excretion of pyridinium crosslinks. J. Bone Miner. Res. 9 (12), 1883–1888.
Starborg, T., Kalson, N.S., Lu, Y., Mironov, A., Cootes, T.F., Holmes, D.F., Kadler, K.E., 2013. Using transmission electron microscopy and 3View to determine collagen fibril size and three-dimensional organization. Nat. Protoc. 8 (7), 1433–1448.
Turner, C.H., Burr, D.B., 1993. Basic biomechanical measurements of bone: a tutorial. Bone 14 (4), 595–608.
Undale, A.H., Drucker, D.J., Moedder, U.I.L., Pursler, M.J., Fraser, D.G., Xiao, J., Khosla, S., Clowes, J.A., 2006. Deletion of glucagon-like peptide-2 receptor leads to marked skeletal deficits in growing mice. In: 28th Annual Meeting of the American Society of Bone and Mineral Research (ASBMR), Philadelphia (PA).
Vashishth, D., 2008. Small animal bone biomechanics. Bone 43 (5), 794–797.
Wichers, M., Schmidt, E., Bidlingmaier, F., Klingmuller, D., 1999. Diurnal rhythm of CrossLaps in human serum. Clin. Chem. 45 (10), 1858–1860.
Xu, B., He, Y., Lu, Y., Ren, W., Shen, J., Wu, K., Xu, K., Wu, J., Hu, Y., 2019. Glucagon like peptide 2 has a positive impact on osteoporosis in ovariectomized rats. Life Sci. 226, 47–56.